Acta Crystallographica Section B
Structural Science
ISSN 0108-7681

Study of the single-crystal X-ray diffuse scattering in paracetamol polymorphs

E. J. Chan* and D. J. Goossens

Research School of Chemistry, Australian National University, Canberra, ACT 0200, Australia

Correspondence e-mail: echanj@rsc.anu.edu.au

Received 26 September 2011
Accepted 2 November 2011

Single-crystal diffuse X-ray scattering from paracetamol polymorphs is successfully calculated with Monte Carlo (MC) models that are used to simulate the crystals. In order to obtain the correct model appropriate force constants are required that describe the interatomic potentials used in the MC algorithm. Coefficients for an empirical 'Buckingham'-type formula are used to determine these force constants. These coefficients are subsequently refined using the least-squares method and are found to converge on similar values for both polymorphic forms. An investigation of the correlation space generated from each model provides what would be expected given that strong displacive correlations exist between the molecules comprising the densely hydrogen-bonded layers. More disordered motions between these layers are present in the model for form (II) as opposed to form (I). An investigation into the peculiarities of librational disorder was also conducted, however, correlation values turn out to be so small that any structural information concerning librational correlation is inconclusive. The purpose of this experiment was to identify if the diffuse scattering features could provide further insight into understanding the physical reasoning behind the metastability of form (II). The form (II) $\rightarrow$ (I) phase transition is also not currently well understood and usually phase transitional information can be obtained from pronounced diffuse scattering features. Since the diffuse scattering is modelled adequately using harmonic potentials it is our conjecture that the 'diffuse' is essentially thermal in origin and does not afford any extra information about the form (II) $\rightarrow$ (I) phase transition.

1. Introduction

Solid-state analyses of the two well known polymorphic forms of paracetamol have been popular since form (II) (orthorhombic) was shown to be better suited to tablet formation (Nichols & Frampton, 1998; Garekani *et al.*, 2000) and was found to have a higher rate of dissolution in water (Boldyreva *et al.*, 2004; Di Martino *et al.*, 1996). Factors concerning the control of its growth and the long-term stability with respect to its conversion to form (I) (monoclinic) are under much investigation (Thomas *et al.*, 2011; Shyam *et al.*, 2009; Drebushchak & Boldyreva, 2004; Burley *et al.*, 2007; Mikhailenko, 2004; Neumann & Perrin, 2009; Oswald *et al.*, 2009). Investigations of the calculated elastic modulus also explain the reason for the better compressibility of form (II) as well as provide criteria for important developments in polymorph prediction (Beyer *et al.*, 2001).

A variety of analytical methods are used to classify and screen the physical properties of solid-state APIs (active pharmaceutical ingredients). These methods often entail many

different crystallization techniques coupled with a very comprehensive combination of calorimetry, microscopy, spectroscopy and of course diffraction (Bernstein, 2002). Owing to the availability of synchrotron sources, observations of the diffuse component (*i.e.* single-crystal diffuse scattering, SCXDS) of the diffracted X-rays from single-crystal structure determination experiments are becoming more prominent and recently investigations into the comparison of the diffuse scattering from polymorphs of molecular crystals has provided great insight into understanding the origin of the underlying behavioral properties of these solids (Chan *et al.*, 2009; Chan & Welberry, 2010; Chan, Welberry, Heerdegen & Goossens, 2010).

The current report describes a comparative analysis of the single-crystal X-ray diffuse scattering from forms (I) and (II) of paracetamol. Diffuse scattering features can often provide information about the behavior of the molecules within crystalline solids (Welberry, 2004; Welberry & Goossens, 2008).

Usual diffraction data obtained for structure solution are the sharp Bragg reflections which are a result of the long-range periodicities in the crystal and their analysis provides the familiar time-and-space average model – a space group and unit cell, occupancies and atomic displacement parameters (ADPs). Structured diffuse scattering is the result of local correlated departures from the average – which is sometimes termed local structure or short-range order. These local structures contain information about molecular environments and conformations, and can be dynamic ('correlated thermal motion') or static in nature (Weber *et al.*, 2001).

Various modelling techniques have been developed for the study of single-crystal X-ray diffuse scattering from molecular crystals. Methods becoming of increasing popularity and efficacy due to advancements in computer power utilize a real-space statistical model of the crystals and Monte-Carlo algorithms (MC) are used to introduce correlated disorder into the model. The diffuse scattering can then be calculated from this model and the calculated data compared with what was observed (Welberry *et al.*, 2001; Welberry, 2000). Very often it is not clear to readers as to why and how a static model for displacive disorder may successfully mimic the disorder from thermal motion. Previous work on the comparison of results from lattice-dynamical models with those obtained from MC methods form the basis of our current investigations (Welberry *et al.*, 1989). In that report the diffuse intensity distribution calculated from the simple lattice-dynamical model was complementary to optical diffraction patterns obtained from MC simulation. Essentially the static model mimics what we would observe from a dynamical model. In our modelling time is not parameterized (this is one of the advantages for using MC) and frequency information is not obtained, but the distributive information will be the same. Statistically the time average and ensemble average are the same and the diffraction experiment by its very nature cannot differentiate between the two.

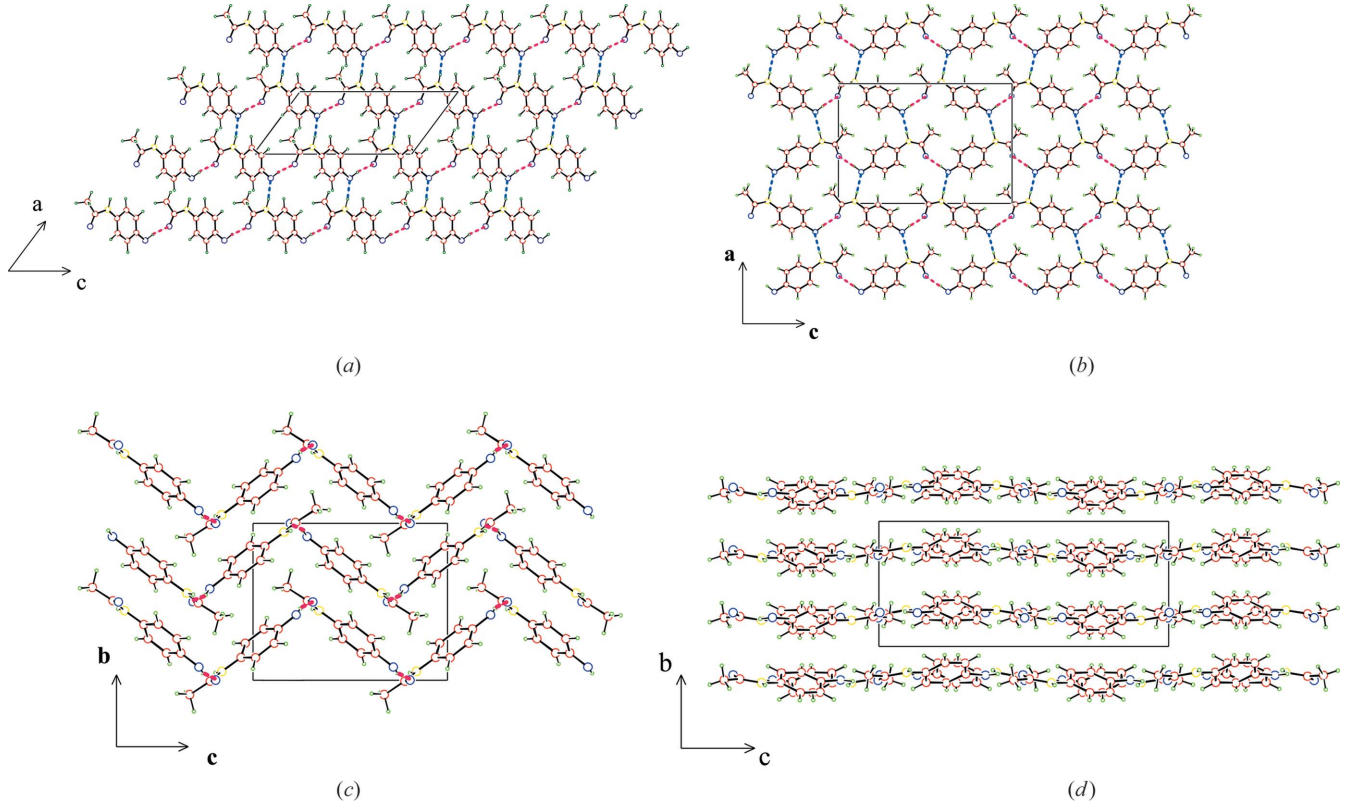

Figure 1
The stacking in a layer of molecules normal to the *b* axis in paracetamol (*a*) form (I) and (*b*) form (II) [note that for form (II), only one layer of the two within a unit cell is shown]. Hydrogen-bonding interactions common to both forms are indicated by dashed lines. View of those layers down the *a* axis for (*c*) form (I) and (*d*) form (II). The planar stacking of layers normal to *b* is clear for form (II).

The current investigation confirms that diffuse scattering for both forms of paracetamol can be well modelled by considering the molecules as rigid bodies with simple harmonic potentials used to approximate the energy associated with a broad range of intermolecular interactions in the crystal [equation (1)]. These potentials serve to correlate the motions of nearby molecules and induce the structured features observed in the diffuse scattering. Recently the idea of using a simple empirical equation [equation (2)] to generate the force constant was explored (Chan, Welberry, Goossens & Heerdegen, 2010). The parameters of this equation then become the parameters of a least-squares refinement, in which χ^2 and its derivatives are calculated *via* 'pixel by pixel' comparison of observed and calculated reciprocal space sections. The strategy requires refinement of only four coefficients. The data fitting procedure uses three reciprocal space basal planes and large portions of the Bragg scattering profile is removed, because it is not calculated by the diffuse scattering calculation. The individual MC simulations are implemented using the program *ZMC* (Goossens *et al.*, 2010). Previous work using this approach has presented correlations amongst positional displacements using polar plots (Goossens *et al.*, 2010). Here, a method for representing correlations amongst orientations of molecules is presented, the intention being to explore the presence of correlated molecular rotations, a phenomenon likely to be required if form (II) is to transform into form (I).

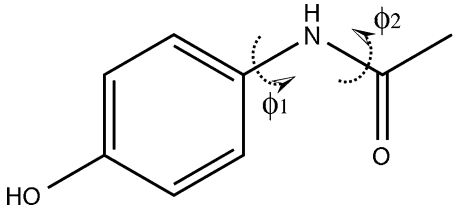

1.1. Description of form (I) and form (II)

Paracetamol molecules stack in both forms as two-dimensional layers made up of end-to-end hydroxyl-H···O-carbonyl hydrogen-bonded ribbons (molecules are related by *c*-glide), which in form (I) stack in the same direction offset by the monoclinic angle as shown in projection down the *b* axis in Fig. 1(*a*). In form (II) these same ribbons stack sequentially in opposing directions (Fig. 1*b*). When viewing the layer stacks horizontally down the *a* axis, it can be seen in form (I) that the layers have an antiparallel herringbone arrangement, whereas in form (II) the layers are planar (Figs. 1*c* and *d*). It is this planar molecular stacking which is the source of much investigation with respect to the ability of form (II) to better undergo plastic deformation during tablet formation.

2. Experimental

All crystals were grown by evaporation at room temperature from ethanol as described in the literature (Haisa *et al.*, 1974, 1976). Crystals of the metastable paracetamol form (II) were very difficult to grow and maintain; often it was found that the crystals had transformed to form (I) during cutting, mounting and data-collection procedures.

2.1. Bragg diffraction experiment

Atomic coordinates derived from the Bragg diffraction experiment are used as the starting point for disorder modelling. Cell parameters for each of the forms are lised in Table 1. The coordinates of form (I) were taken from a 250 K neutron scattering experiment reported by Wilson (2000). Since the previous characterization for the average structure of the orthorhombic form (II) is dated in the 1970s, Bragg data for an average structure were recollected for form (II) and a better *R*-factor resolved. The Bragg data set was collected from a crystal taken from the same batch as the form (II) samples used for diffuse scattering experiments, and a reliable starting set of coordinates for the disorder modelling was obtained. For ease of structural comparison between the two forms the atomic coordinates for form (I) are placed in a non-standard setting of $P2_1/c$ with an acute β angle. This was obtained by using the transformation matrix [0 0 1][0 −1 0][1 0 2], which corresponds to $x, y, z \rightarrow z, -y, x + 2z$ on the original coordinates from the $P2_1/a$ setting. Form (II) is placed in the standard orthorhombic setting of *Pbca*. In this setting molecular layers which are normal to *b* will coincide directly to analogous layers with the chosen form (I) setting.

The submitted CIF file corresponds to form (II) in the above standard setting and contains details of the refinement. The CIF and Bragg reflection data are available as supplementary material.[1]

2.2. Diffuse scattering experiment

All data were collected at room temperature using a mar345 image plate. Data for forms (I) and (II) of paracetamol were collected on the powder diffraction beamline at the Australian Synchrotron. Here the photon energy was 17 Kev [λ = 0.7000 (1) Å], the detector distance was 120.0 mm for form (I) and 130.0 mm for form (II). Exposure times were 15 s per frame for form (I) and 60 s per frame for form (II). Further details of the data collection methods and reciprocal space reconstruction have been described in a previous report (Chan *et al.*, 2009).

2.3. Simulation details and calculation of diffuse intensities

MC models used to calculate diffuse scattering consist of an array of 48 × 48 × 48 unit cells, each of which initially contains atomic coordinates taken from the Bragg structure as mentioned in the previous section. Correlated displacements are generated using the program *ZMC* (Goossens *et al.*, 2010).

Intermolecular atom···atom interactions are modelled as springs, and intermolecular rigid-body rotations around single bonds as torsional springs. More specifically, the acceptance/rejection criteria for the position of a molecule in the model

[1] Supplementary data for this paper are available from the IUCr electronic archives (Reference: EB5012). Services for accessing these data are described at the back of the journal.

Table 1
Values for form (I) were taken from a previous report (Wilson, 2000) and have been appropriately transformed (see text for details).

Parameters	Form (I) ($P2_1/c$)	Form (II) ($Pbca$)
a	7.0860 (7)	11.8237 (4)
b	9.3150 (9)	7.3971 (3)
c	14.4349 (14)	17.1526 (7)
α	90.000	90.000
β	53.298 (5)	90.000
γ	90.000	90.000
D_x (g cm^{-3})	1.314	1.339

crystal is based on minimizing the energy which is calculated using equation (1)

$$E_{\rm therm} = \sum_{\substack{\text{all linear}\\ \text{springs}}} K_i(d - d_0)^2 + \sum_{\substack{\text{torsional}\\ \text{springs}}} G_{\rm t}(\varphi - \varphi_0)^2, \qquad (1)$$

where K_i are force constants and $(d - d_0)$ is the difference between the actual (d) and average (d_0) atom$\cdots$atom distance. The values of the second term ($G_{\rm t}$, φ and φ_0) are analogous to those of the atom$\cdots$atom term, except that they correspoond to torsional springs. Previous work on form (I) of paracetamol suggests an empirical exponential function can be used to calculate the force constants based on intermolecular distances in the average structure (Chan, Welberry, Goossens & Heerdegen, 2010). Equation (2) is adopted because the exponential decay is analogous to that of the Buckingham potentials used in calculations for crystal structure prediction (Day *et al.*, 2005; Filippini & Gavezzotti, 1993). The workings of this approximation are best explained in previous reports (Chan, Welberry, Goossens & Heerdegen, 2010). A, B and C are the coefficients for an exponential decay curve, K_i is the force constant and $r^{\rm vdw}$ is the van der Waals radius

$$K_i = A\exp\left(B\left(d_0 - \sum_{\rm atoms} r^{\rm vdw}\right)\right) - C. \qquad (2)$$

Torsional force constants to represent the rotational degrees of freedom φ_1 and φ_2 shown in the chemical scheme are all assigned the same value (G_t).

Diffuse scattering for the basal reciprocal space sections is calculated using the program *DIFFUSE* (Butler & Welberry, 1992). It should be noted that all calculated patterns contain no Bragg peaks.

2.4. Least-squares refinement of form (I) and form (II) data

The quantitative least-squares fitting is based on a pixel-by-pixel refinement procedure (Welberry *et al.*, 1989) where the quantity minimized is $\chi^2 = \sum w(I_{\rm obs} - I_{\rm calc})^2$. This corresponds to an agreement factor $R = \sum w(I_{\rm obs} - I_{\rm calc})^2/\sum wI_{\rm obs}^2$ with weights (w) given by $1/(I_{\rm obs})^{1/2}$. In previous methods spring constants were refined as separate parameters, however, in this study three parameters are used for approximating the force constants and one global parameter for internal molecular degrees of freedom [equation (2)].

A total of 136 322 pixels from the three basal planes were used in the fit for form (I) and 171 490 were used for form (II).

Table 2
Values for parameters of equation (2) from least-squares refinements.

	A	B	C	$G_{\rm t}$
Form (I)	11 (1)	−0.42 (5)	−8.1 (7)	18 (4)
Form (II)	11 (1)	−0.42 (4)	−8.1 (6)	22 (1)

1000 MC simulation cycles were used to bring the models into thermal equilibrium.

The empirical 'Buckingham'-like formulation [(equation 2)] allows an arbitrary number of intermolecular springs to be controlled by only 3 parameters. In many cases the total number of spring types (non-symmetry equivalent springs, or interactions) required for modelling can be a few hundred and this increases with the size of the molecules in the simulation and also with the amount of static disorder. Hence this is a large reduction in the number of free parameters. The central complexity that this approach tackles is that unit cells cannot be considered as identical when exploring local ordering. The fact that the interactions do not vary from cell to cell is the reason for using the MC approach, in which a limited set of interactions (and therefore parameters) are used to generate a large (of the order of 10^6) number of atomic coordinates, thus making modelling of the diffuse scattering practicable. The approach used here can be thought of as a further abstraction, in that the parameters of the fit are now those used to derive the force constants from which the atomic coordinates are in turn derived.

Starting values for A, B, C and $G_{\rm t}$ were determined manually through successive qualitative trials: $A = 10$, $B = -0.5$, $C = -8.5$ and $G_{\rm t} = 20$. The shifts used to increase(decrease) these values in the refinement were $\delta A = 1.0$, $\delta B = 0.1$, $\delta C = 0.1$ and $\delta G_{\rm t} = 5$. By performing MC simulations on an initial set of values, and on a series of simulations in which one of these variables was increased (decreased), an estimate of the dependence of the goodness-of-fit on the parameter values could be obtained, allowing a least-squares matrix to be constructed and a new set of variable values determined. All atom$\cdots$atom contacts of < 4 Å were generated for the simulations, giving 175 intermolecular contacts for form (I) and 172 for form (II).

3. Comparison of observed and calculated diffuse scattering data

Although full three-dimensional data were collected, the observed data used in each of the refinements were reconstructions of the basal sections. Adequate corrections were made for scattering artifacts as described in previous literature (Welberry *et al.*, 2005).

The current methodology for this investigation differs from that reported in previous literature where small boxes encompassing particular diffuse features taken from these section were used in the refinement (Chan *et al.*, 2009; Beasley *et al.*, 2008; Welberry *et al.*, 1998). In the current report, refinement of full sections was used. The calculated data was scaled and background corrections made.

Table 3
Agreement factors R corresponding to Fig. 4.

Values are shown for comparative trials from both forms (I) and (II). The label in the experiment column is a cross-reference to the experimental descriptions provided in the caption to Fig. 4. Please note that Fig. 4 shows graphical results only for form (II) and not for form (I).

Experiment	Form (I) ($P2_1/c$)	Form (II) ($Pbca$)
Fig. 4(*a*)	0.178	0.123
Fig. 4(*c*)	0.194	0.130
Fig. 4(*b*)	0.177	0.124
Fig. 4(*d*)	0.180	0.125

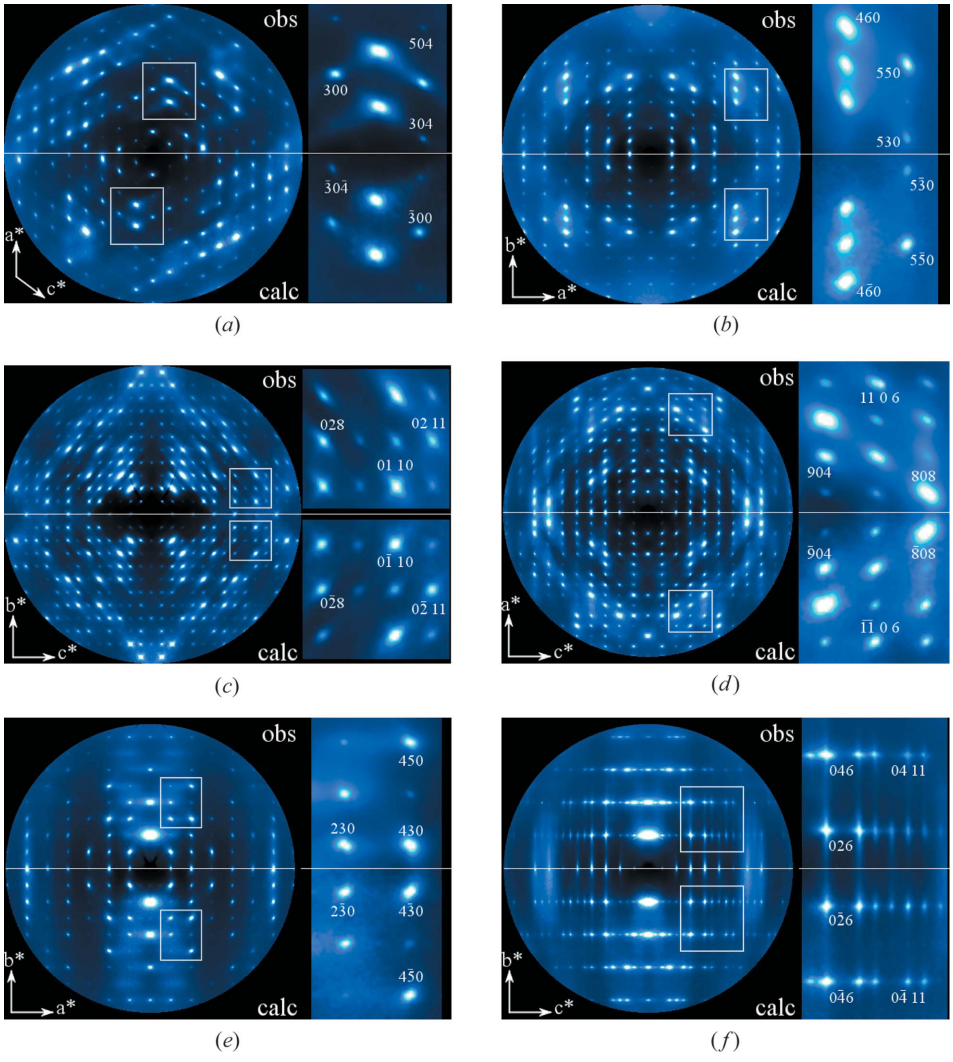

Figure 2
Comparison of observed and calculated diffraction patterns for both forms (I) and (II) of paracetamol. In all figures the upper and lower half-circles represent the observed and calculated diffuse diffraction patterns for a basal section of reciprocal space. (*a*), (*b*) and (*c*) are respectively the *h*0*l*, *hk*0 and 0*kl* basal sections for form (I) and (*d*), (*e*) and (*f*) are the same sections for form (II). The direction of the reciprocal axis also corresponds to the packing diagrams in Fig. 1. Observed and calculated images have a scaling and background correction applied as required. Bragg peaks are omitted from the calculated images. Diffraction sections are calculated from models in which the parameters corresponding to equation (2) were refined using the automated least-squares procedure described in §2.4. The number of MC cycles used for each simulation during the automated refinement is 1000, however, for the images shown 10 000 cycles are used to reproduce sharper diffraction features.

3.1. Results of the least-squares refinement

Automated refinement of coefficients in (2) was found to converge after 12 cycles of refinement; the refined values are listed in Table 2. A comparison of observed and calculated diffuse scattering patterns for both forms is shown in Fig. 2. Additional $hk(h+1)$ layers are shown in Fig. 3 illustrating the predictive power of the model parameters fitted manually and then with subsequent least-squares refinement only from basal sections. It was noticed that even though the agreement factors were reasonable, certain sharper scattering features were not present in the calculated diffuse scattering unless the number of MC cycles for the simulation was increased to 10 000. Hence 1000 cycles were used in the refinement, and then the optimized model was run for 10 000 cycles for final evaluation. A comparison of the difference between the calculated scattering features for these changes in the number of cycles is shown for form (II) in Fig. 4 as well as all the corresponding R factors for both forms listed in Table 3. Even though the calculated diffuse scattering features better resemble those observed when the larger number of MC cycles is used the R factor that is calculated is slightly higher. This is a common indication that many other factors need to be considered when making objective conclusions on structural models based entirely on agreement factors derived in the process of quantitative diffuse scattering analysis.

3.2. Correlating intramolecular dihedral angles

Once the parameters for the curve [equation (2)] and G_t were fitted using least-squares, diffraction patterns were calculated from simulations in which a cross-term was added to force correlation of the dihedral angles φ_1 and φ_2 within a molecule (as indicated by the chemical scheme in §1). Similar calculations were made in previous work for *p*-(*N*-methylbenzylidne-*p*-methylaniline; Beasley *et al.*, 2008) and an in-depth description of what these forces represent is given in Goossens *et al.* (2010). This test was performed for both forms (I) and

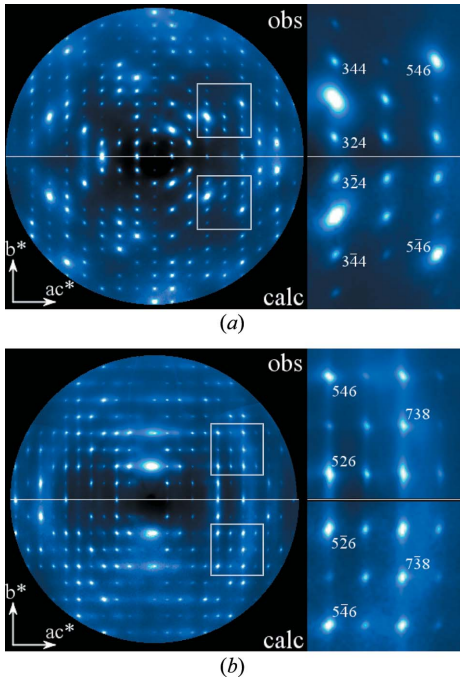

Figure 3
Comparison of observed and calculated diffraction patterns in the $hk(h+1)$ layer for (*a*) form (I) and (*b*) form (II). The images are still representative of the same procedures described for the images shown in Fig. 3, but these are examples of non-basal reciprocal space sections and the resemblance between the observed and calculated represents the accuracy of the model even though the manual and subsequent least-squares fitting of parameters was restricted to basal sections.

(II) of paracetamol, however, calculated diffraction patterns for these simulations are shown only for form (II) in Fig. 4. The corresponding agreement factors (R) for each of these tests were also calculated for both forms (I) and (II), and are listed in Table 3. In calculating the agreement factors for this particular test no automated refinement procedure was performed and the R factors shown are based on the residuals from a single simulation where either a positive or negative value for the correlation was used. It can be seen from the results that conclusions in support of the direct correlation between dihedral angles are not substantiated by diffuse features. That is not to say that these two angles do not show evidence of correlation (they show a correlation coefficient of −0.21), but that this correlation arises from the network of contact vectors rather than through direct interaction; given that φ are adjacent on the molecule, it is clear that as far as contact vectors connecting with atoms in the O—C—CH_3 group are concerned, 'stretching' of contacts due to rotation around φ_1 will, to a small extent, be cancelled out by a counter-rotation around φ_2.

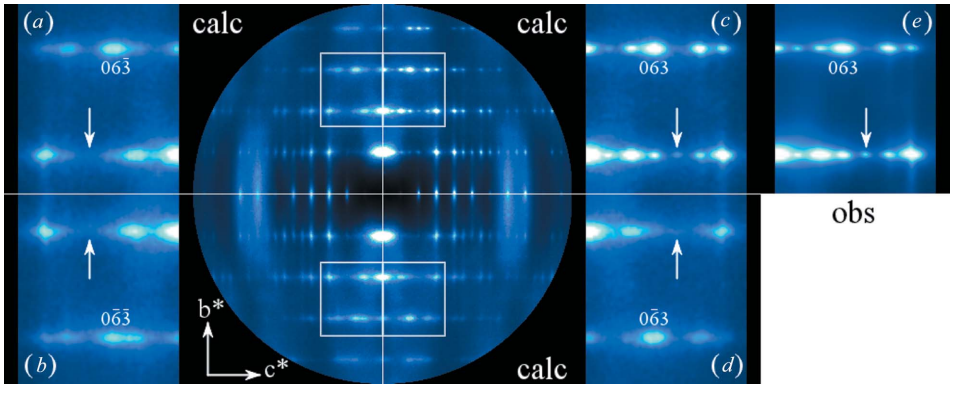

Figure 4
Representative sections of the 0*kl* diffraction pattern for form (II) of paracetamol (*a*)–(*d*) are calculated from different simulations (see text) and (*e*) is the observed reconstruction provided for comparison. In all patterns a white arrow indicates a particularly sharp diffuse feature. For all models the force constants for intermolecular potentials are derived from the automated refinement described in §3.1. (*a*) is calculated from a simulation that is equilibrated across 1000 MC cycles, whereas (*c*) is calculated from a model that had 10 000 cycles. The position of the white arrow shows that the sharp feature could not be reproduced unless the number of MC cycles for the simulation was high. (*b*) is calculated from a model where the torsional angles for the molecule (φ_1 and φ_2) were positively correlated, whereas (*d*) is representative of the corresponding negative correlation.

4. Interpretation of the models

4.1. Displacement correlations

The use of displacement correlation diagrams (referred to as 'peanut diagrams' in some works; Chan *et al.*, 2009) to investigate the correlation space from current harmonic models is well established. One such diagram is calculated as follows:

(i) A direction in space is selected. For Fig. 5(*a*), this would be a direction in the *ac* plane. This direction may be parametrized by an angle, θ, the angle to the horizontal axis (in this case, *c*).

(ii) The projection of the displacements of the origin of two molecules of interest onto this direction are obtained, call these $\delta_1(\theta)$ and $\delta_2(\theta)$.

(iii) This is repeated for many pairs of molecules, all pairs of the same 'type'.

(iv) The correlation between $\delta_1(\theta)$ and $\delta_2(\theta)$ is calculated; call this $\rho(\theta)$.

(v) The value of θ is incremented and the process repeats.

The end result is a function, $\rho(\theta)$, that can be plotted in polar coordinates and represents the degree of correlation of the components of the molecular displacements for selected pairs of molecules. In Fig. 5 this process is performed not (necessarily) for first-neighbor molecules but for symmetry-equivalent molecules separated by various unit-cell translations, showing how the displacement correlations are structured as a function of separation of the molecules. The diagram boxed in Fig. 5(*a*) shows the scale of these plots – correlations extend out to 0.2, and are in this case always positive in sign.

Fig. 5(*a*) is a diagram of the correlation space in form (I) which corresponds to the projection down *b* in Fig. 1(*a*). In Fig. 1 hydrogen-bonding motifs shown as dotted lines usually represent strong interactions between molecules which stack as layers normal to the *b* axis. The correlation diagram clearly shows strongly correlated displacements for the packing of molecules in the [100] and [$\bar{2}$01] directions. It can be seen that the direction of the strongest correlation does not necessarily coincide in the direction of any of the hydrogen bonds if they are represented as vectors in the lattice, however, the molecules that pack in the direction of the strongly correlated displacements in [$\bar{2}$01] are still linked by the same N—H···H—O hydrogen bonds which are normal to the (100) plane. Fig. 5(*b*) shows the corresponding correlation diagram for the stacking projection down *a* (Fig. 1*c*). The antiparallel stacking for form (I) layers normal to the *b* axis and the herringbone-like stacking give rise to the characteristic 'peanut' shapes at approximately 45° on the molecules related by [011] for example.

The effect on correlated displacements for the *a* glide-related stacking of chains of molecules along the *c* axis in the molecular layers normal to the *b* axis in form (II) (see Fig. 1*b*) can be seen in the correlation plots in Fig. 5(*c*) and compared with that of form (I). The antiparallel stacking of molecular chains gives rise to correlated displacements in the layer shown to be more isotropic for form (II) than for form (I) – [10$\bar{1}$] and [101] are much more similar here than in Fig. 5(*a*). The diagram in Fig. 5(*d*) indicates strong correlations between neighbors in both the [010] and [001] directions, which is surprising since it might have been expected that the parallel stacking of layers of molecules normal to the *b* axis would mean that the correlated displacements observed in the *b* direction would be significantly smaller than those in the *c* direction. Recalling that $|c| > \sim 2|b|$ suggests that it is more appropriate to compare the [001] diagram with [020], which is seen to be smaller. This indicates that as a function of molecular separation, correlations of motions in the *c* direction are stronger for molecules packing along the *c* direction than the correlation of *b*-direction motions for molecules packed along *b* (the correlation of longitudinal motions).

Also the diagram for [010] shows weak correlation in the *c* direction (molecular displacements transverse to the intermolecular vector), indicating there are disordered displacements between the layers that pack in the *b* direction. In other words, they can slip relative to each other. This is reinforced by the pronounced weakness of any correlations not along the principal directions, indicating (as might be expected) that this structure is very susceptible to shear parallel to the *ac* plane. Indeed, this is a key difference between the forms – the correlations between [010] neighbors in the *bc* plane of form (I) (Fig. 5*b*) are relatively strong both in *c* and *b*, and similarly for *a* and *c* correlations in the *ca* plane for *both* polymorphs (Figs. 5*a* and *c*). It is only in the *bc* plane of form (II) that the anisotropy in the correlation structure is so apparent, indicating that the crystal can be considered as a series of *ac* layers that can easily slide past each other. This may have significance

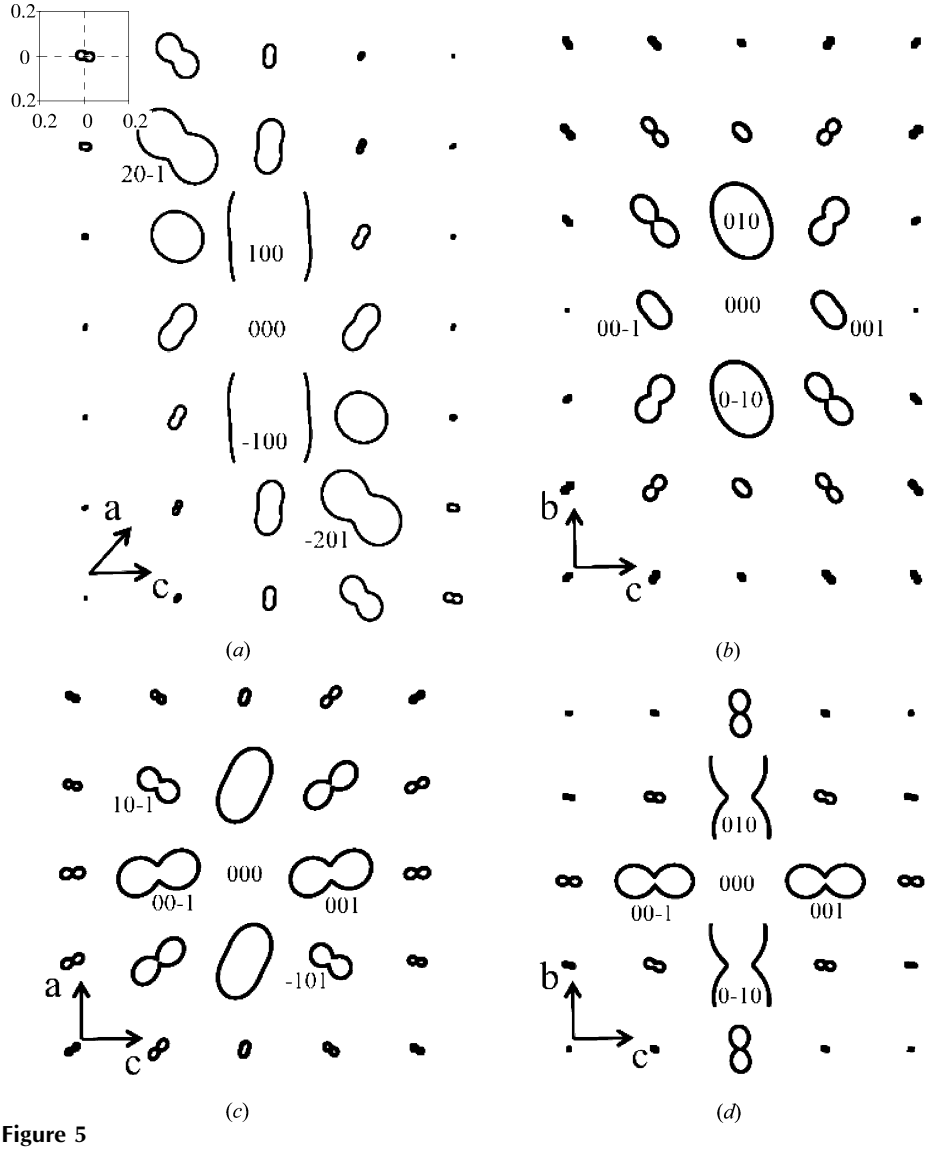

Figure 5
Displacement correlation ('peanut') diagrams calculated from the models for forms (I) and (II) (see text for details). For all models the force constants for intermolecular potentials were derived from an automated refinement as described in §2.4. (*a*) and (*b*) correspond to *ac* and *bc* planes for form (I). (*c*) and (*d*) correspond to *ac* and *bc* planes for form (II).

both for the solubility behavior of form (II) and also the transformation to form (I).

It can be noted that for form (II), when examining the correlations amongst the molecular variables for a single molecule, the *a* and *c* coordinates show a small correlation (~ 0.14), which may not appear significant (although with over 12 000 molecules contributing to the calculation, it can be reliably considered to differ from zero). Conversely, the correlations involving the *b* coordinates are both smaller than 0.04, agreeing with the idea that the molecules move in *ac* sheets. For form (I), only the correlation between *a* and *b* coordinates is approximately zero, with the *b* coordinate showing some correlation with *c* (~ -0.11) agreeing with the idea that the structure is more cohesive.

It is also not surprising that upon close inspection of values documented for elasticity constants (Beyer *et al.*, 2001), we find an agreement with at least the more pronounced diffuse scattering features observed for form (II), namely the streaking along b^* [see Table 2 of that reference and please note that the 'slip'-layer stacking direction for form (II) in that report is the *c* direction and in our report it is the *b* direction]. Since the diffuse scattering is of thermal origin it is related to the elasticity tensor. Those streaking features along b^* we attribute to disordered displacements for molecules stacking between 'slip' planes. This coincides with the relatively lower values found for the elastic constant C33 with respect to the other axial elastic constants and also the lower relative values for shear elastic constants C44 and C55.

Low-frequency Raman and other vibrational spectra are strongly related to thermal diffuse scattering. However, our MC modelling described does not take into account the vibrational motion of the proton between acceptor and donor, which appears to be related to the hydrogen-bond vibrational disorder revealed by Raman scattering (Kolesov *et al.*, 2011).

It has been observed that the O···H—O bonds are more disordered for form (I) than for form (II) and the N—H···O bonds are more disordered for form (II) than form (I) (Kolesov *et al.*, 2011). The correlation plots shown here show motions that result from a large cooperative network of intermolecular interactions. These plots imply that packing of the crystal structures may be the origin of the disorder that is observed in the Raman studies. For example, the modelling shows strongly disordered displacements along neighboring molecules packing through the N—H···O hydrogen bonds in form (II) as opposed to the molecules that pack through O—H···O bonds. Further, in the form (I) model neighboring molecules related by the N—H···O hydrogen bonds are in fact more strongly correlated than those neighbors related by the O—H···O hydrogen bond. This agrees with the results from Raman spectroscopy (Kolesov *et al.*, 2011). The reasoning behind this is that when we observe in our model less displacement correlation associated with neighbors connected through a specific D—H···A then we may postulate that this D—H stretching frequency would be softer than a D—H stretching frequency for D—H···A associated with neighbors that are strongly correlated to displacement. This is because there would be more degrees of mechanical freedom for the former hydrogen due to outcomes from the crystal packing.

To explore what further structural information concerning the form (II) → (I) phase transition may be afforded from this model, the correlations amongst the molecular orientations were explored since molecules would need to re-orient themselves from the planar stacks in form (II) to the anti-parallel stacks in form (I), and this would require rotational motions of the molecules in the lattice. However, it was found that neither the overall molecular orientation nor the torsion angles showed any substantial correlation between molecules.

5. Conclusions

Diffuse data for both polymorphic forms of paracetamol have been fitted using a MC model for the crystal. There is no strong signal in the data of the metastability of form (II), other than evidence for the ease of shearing of the crystal in directions parallel to the *ac* plane. Based on previous work the diffuse scattering in form (II) may have been expected to require more complex methods of modelling such as in recent studies of aspirin and benzocaine (Chan, Welberry, Heerdegen & Goossens, 2010; Chan & Welberry, 2010). This, however, was not the case – there was no strong evidence of anharmonicity for example, and there is no indication of any underlying phase transitional behavior that can be derived from the diffuse scattering collected from a crystal of form (II).

The disorder associated with displacement correlations between molecules associated with these bonds may not necessarily substantiate an effect on solid-state stability, however, correlated motion can often be reflective of this. For example, in our work on benzocaine (Chan & Welberry, 2010) both polymorphic forms showed strong correlated motion. However, the form that undergoes the phase transformation possesses an alternative low-energy phase not too far away in terms of atom shifts, whereas the shifts required to transform form (I) to form (II) of paracetamol are quite significant. Given the variability of 'shelf' life for form (II), it may be that effects of trapped solvent, not accounted for in a model such as that presented here, may be important.

The mechanical models indicate that it is the packing of the form (II) structure that facilitates disorder of the intermolecular displacements between the strongly hydrogen-bonded layers. This supports the idea that the stability between structures is a cumulative effect of all intermolecular interactions (not just hydrogen bonds). We infer that simple considerations of packing arrangements *e.g.* layer packing *versus* the herringbone packing are often the source for differences in stability between polymorphic forms. It would indeed seem that form (II) should be less stable than form (I), yet from our work insight is not obtained into whether this difference in stability is sufficient enough to explain the transformation from form (II) to form (I).

Use of an empirical approximation for the intermolecular potentials has worked well for this and previous molecular systems that have a large density of hydrogen bonds (*i.e.*

aspirin and paracetamol polymorphs). This may not necessarily be so for molecular crystals that have a much lower density of hydrogen bonds. In previous work involving 6-exp potentials (Filippini & Gavezzotti, 1993), there is a significant difference between the values of coefficients required for different classes of intermolecular bonding densities in order to better approximate lattice energies. Further investigation into this method of approximation is currently at hand.

The support of the Australian Research Council, the Australian Partnership for Advanced Computing and the Australian Synchrotron Research Program are gratefully acknowledged. DJG gratefully acknowledges the support of the Australian Institute of Nuclear Science and Engineering, Dr Kia Wallwork from the powder diffraction beamline for assistance with the collection of the diffuse scattering data, and Dr Aidan Heerdegen for help with data reduction and computing support.

References

Beasley, A. G., Welberry, T. R., Goossens, D. J. & Heerdegen, A. P. (2008). *Acta Cryst.* B**64**, 633–643.
Bernstein, J. (2002). *Polymorphism in Molecular Crystals*. Oxford University Press.
Beyer, T., Day, G. M. & Price, S. L. (2001). *J. Am. Chem. Soc.* **123**, 5086–5094.
Boldyreva, E. V., Drebushchak, V. A., Paukov, I. E., Kovalevskaya, Y. A. & Drebushchak, T. N. (2004). *J. Therm. Anal. Calorim.* **77**, 607–623.
Burley, J. C., Duer, M. J., Stein, R. S. & Vrcelj, R. M. (2007). *Eur. J. Pharm. Sci.* **31**, 271–276.
Butler, B. D. & Welberry, T. R. (1992). *J. Appl. Cryst.* **25**, 391–399.
Chan, E. J. & Welberry, T. R. (2010). *Acta Cryst.* B**66**, 260–270.
Chan, E. J., Welberry, T. R., Goossens, D. J. & Heerdegen, A. P. (2010). *J. Appl. Cryst.* **43**, 913–915.
Chan, E. J., Welberry, T. R., Goossens, D. J., Heerdegen, A. P., Beasley, A. G. & Chupas, P. J. (2009). *Acta Cryst.* B**65**, 382–392.
Chan, E. J., Welberry, T. R., Heerdegen, A. P. & Goossens, D. J. (2010). *Acta Cryst.* B**66**, 696–707.
Day, G. M. *et al.* (2005). *Acta Cryst.* B**61**, 511–527.
Di Martino, P., Guyot-Hermann, A. M., Conflant, P., Drache, M. & Guyot, J. C. (1996). *Int. J. Pharm.* **128**, 1–8.
Drebushchak, T. N. & Boldyreva, E. V. (2004). *Z. Kristallogr.* **219**, 506–512.
Filippini, G. & Gavezzotti, A. (1993). *Acta Cryst.* B**49**, 868–880.
Garekani, H. A., Ford, J. L., Rubinstein, M. H. & Rajabi-Siahboomi, A. R. (2000). *Int. J. Pharm.* **208**, 101–110.
Goossens, D. J., Heerdegen, A. P., Chan, E. J. & Welberry, T. R. (2010). *Metall. Mater. Trans. A*, **42**, 23–31.
Haisa, M., Kashino, S., Kawai, R. & Maeda, H. (1976). *Acta Cryst.* B**32**, 1283–1285.
Haisa, M., Kashino, S. & Maeda, H. (1974). *Acta Cryst.* B**30**, 2510–2512.
Kolesov, B. A., Mikhailenko, M. A. & Boldyreva, E. V. (2011). *Phys. Chem. Chem. Phys.* **13**, 14243–14253.
Mikhailenko, M. A. (2004). *J. Cryst. Growth*, **265**, 616–618.
Neumann, M. A. & Perrin, M.-A. (2009). *CrystEngComm*, **11**, 2475–2479.
Nichols, G. & Frampton, C. S. (1998). *J. Pharm. Sci.* **87**, 684–693.
Oswald, I. D. H., Chataigner, I., Elphick, S., Fabbiani, F. P. A., Lennie, A. R., Maddaluno, J., Marshall, W. G., Prior, T. J., Pulham, C. R. & Smith, R. I. (2009). *CrystEngComm*, **11**, 359–366.
Shyam, K., Tomislav, F., Fábián, L., Laity, P. R., Day, G. M. & Jones, W. (2009). *Adv. Mater.* **21**, 3905–3909.
Thomas, L. H., Wales, C., Zhao, L. & Wilson, C. C. (2011). *Cryst. Growth Des.* **11**, 1450–1452.
Weber, T., Estermann, M. A. & Bürgi, H.-B. (2001). *Acta Cryst.* B**57**, 579–590.
Welberry, T. R. (2000). *Acta Cryst.* A**56**, 348–358.
Welberry, T. R. (2004). *Diffuse X-ray Scattering and Models of Disorder.* Oxford University Press.
Welberry, T. R. & Goossens, D. J. (2008). *Acta Cryst.* A**64**, 23–32.
Welberry, T. R., Goossens, D. J., Edwards, A. J. & David, W. I. F. (2001). *Acta Cryst.* A**57**, 101–109.
Welberry, T. R., Goossens, D. J., Heerdegen, A. P. & Lee, P. L. (2005). *Z. Kristallogr.* **222**, 1052–1058.
Welberry, T. R., Hua, G. L. & Withers, R. L. (1989). *J. Appl. Cryst.* **22**, 87–95.
Welberry, T. R., Proffen, Th. & Bown, M. (1998). *Acta Cryst.* A**54**, 661–674.
Wilson, C. C. (2000). *Z. Kristallogr.* **215**, 693–701.